Weierstraß-Institut
für Angewandte Analysis und Stochastik
Leibniz-Institut im Forschungsverbund Berlin e. V.

Preprint ISSN 2198-5855

Efficient coupling of electro-optical and heat-transport models for broad-area semiconductor lasers

Mindaugas Radziunas[1], Jürgen Fuhrmann[1], Anissa Zeghuzi[2],

Hans-Jürgen Wünsche[1,2], Thomas Koprucki[1], Carsten Brée[1], Hans Wenzel[2],

Uwe Bandelow[1]

submitted: December 7, 2018

[1] Weierstrass Institute
Mohrenstr. 39
10117 Berlin
Germany
E-Mail: mindaugas.radziunas@wias-berlin.de
juergen.fuhrmann@wias-berlin.de
hans-juergen.wuensche@wias-berlin.de
thomas.koprucki@wias-berlin.de
carsten.bree@wias-berlin.de
uwe.bandelow@wias-berlin.de

[2] Ferdinand-Braun-Institut
Leibniz Institut für Höchstfrequenztechnik
Gustav-Kirchhoff-Str. 4
12489 Berlin
Germany
E-Mail: anissa.zeghuzi@fbh-berlin.de
hans.wenzel@fbh-berlin.de

No. 2558
Berlin 2018

2010 *Mathematics Subject Classification.* 65Z05, 78A60, 80A20, 78M12, 78M34, 65N08.

2010 *Physics and Astronomy Classification Scheme.* 42.55.Px, 44.05.+e, 02.30.Jr, 02.60.Lj, 02.70.Dh.

Key words and phrases. Broad area lasers, modeling, traveling wave, current spreading, heat transport, iterative coupling, different time scales, finite volumes, efficient implementation.

This work is supported by the German Federal Ministry of Education and Research contract 13N14005 as part of the EffiLAS/HotLas project and by the EUROSTARS Project E!10524 HIP-Lasers.

Edited by
Weierstraß-Institut für Angewandte Analysis und Stochastik (WIAS)
Leibniz-Institut im Forschungsverbund Berlin e. V.
Mohrenstraße 39
10117 Berlin
Germany

Fax: +49 30 20372-303
E-Mail: preprint@wias-berlin.de
World Wide Web: http://www.wias-berlin.de/

Efficient coupling of electro-optical and heat-transport models for broad-area semiconductor lasers

Mindaugas Radziunas, Jürgen Fuhrmann, Anissa Zeghuzi, Hans-Jürgen Wünsche, Thomas Koprucki, Carsten Brée, Hans Wenzel, Uwe Bandelow

Abstract

In this work, we discuss the modeling of edge-emitting high-power broad-area semiconductor lasers. We demonstrate an efficient iterative coupling of a slow heat transport (HT) model defined on multiple vertical-lateral laser cross-sections with a fast dynamic electro-optical (EO) model determined on the longitudinal-lateral domain that is a projection of the device to the active region of the laser. Whereas the HT-solver calculates temperature and thermally-induced refractive index changes, the EO-solver exploits these distributions and provides time-averaged field intensities, quasi-Fermi potentials, and carrier densities. All these time-averaged distributions are used repetitively by the HT-solver for the generation of the heat sources entering the HT problem solved in the next iteration step.

1 Introduction

High-power (HP) edge-emitting broad-area semiconductor lasers (BALs) [Fig. 1(a)] are important light sources due to their numerous applications [1]. Accurate modeling and simulation of BALs are critical for improving their performance or for the evaluation of novel design concepts [2]. Since the emission of BALs usually has an irregular spatiotemporal dynamics, the adequate modeling of the optical fields in BALs should account for the time and at least two spatial (longitudinal and lateral) coordinates. Fig. 1(b) gives a schematic representation of the domain where such an electro-optical (EO) model of BALs should be defined. This domain can be interpreted as a projection of the whole diode (panel (a) of the same figure) to the active zone of the diode consisting of a single or several quantum wells (QWs).

For a proper recovery of the essential emission characteristics in HP BALs operated in continuous-wave (CW) mode, the self-heating-induced change of the refractive index plays a crucial role and cannot be ignored. Due to extremely different time scales (femto- and picoseconds for optical fields, nanoseconds for carrier densities, and microseconds for thermal effects), fully comprehensive dynamic simulation of arbitrary HP BALs is hardly possible. For this reason, the majority of BAL solvers rely on differently reduced models. For example, partial-differential equation models that are steady in time and two- or three- dimensional in space are used for the simulation of special laser devices operating in steady-state (master-oscillator power-amplifier lasers, [3]), or the analysis of stable optical modes close to threshold [4]. Models with eliminated longitudinal dependence have also been used to analyze the optical modes and their dynamics [5, 6].

In our previous work on the dynamics of BALs and tapered BALs [7, 8, 9], we were exploiting a 1 (time) + 2 (space) dimensional EO model and solver `BALaser` [10], that has been recently extended by an inhomogeneous current-spreading (CS) solver [11, 12]. Thermal effects were represented by a linear dependence of the wavelength tuning on the injected current [7, 8] or by a fixed externally estimated thermal contribution to the spatial distribution of the refractive index [9]. Recently, we have demonstrated that our EO solver iteratively coupled to an external steady heat transport (HT) solver used to simulate thermal distributions within several lateral-vertical laser cross-sections [see Fig. 1(c)] can reproduce the experimentally observable narrowing of the near fields in HP BALs [13]. In particular,

DOI 10.20347/WIAS.PREPRINT.2558 Berlin 2018

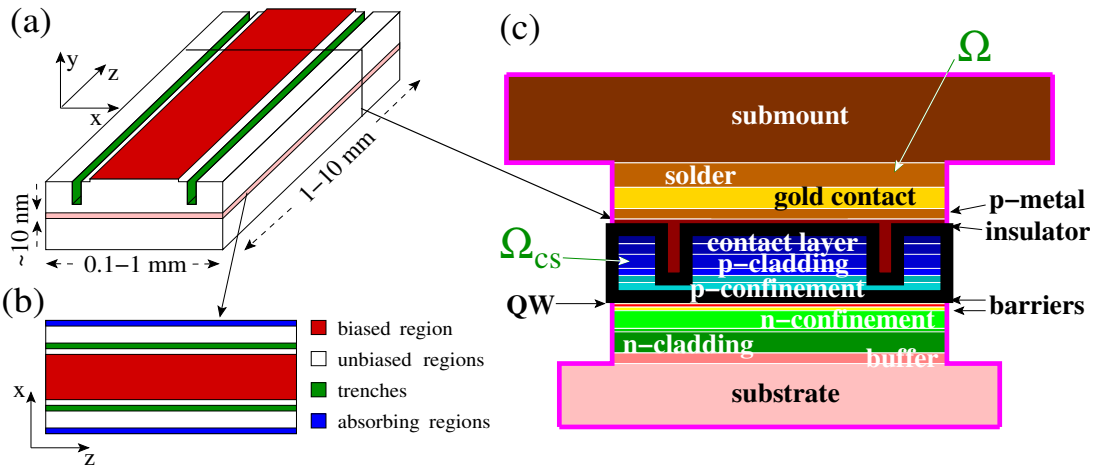

Figure 1: Schematic representation of an edge-emitting broad-area laser (a), its projection to the active zone (b), and the transverse cross-section Ω (c), where the heat-transport and the inhomogeneous current-spreading (thick black-framed region Ω_{cs}) problems are solved.

these simulations have shown that for a proper estimation of the spatial emission quality we should take into account not only a thermally-induced lateral but also a longitudinal variation of the refractive index distribution. In this paper, we briefly introduce our EO and HT models and discuss the realization of the iterative coupling between corresponding in-house developed solvers.

This paper is organized as follows. In Section 2 we give a brief description of the EO model equations. The following Section 3 discusses the HT model and its simplification. Section 4 gives a brief overview of numerical algorithms used to solve the EO- and HT- models and explains an iterative coupling between the corresponding solvers. Finally, Section 5 presents and discusses as an example the simulation of a typical BAL device.

2 Electro-optical model

For modeling the nonlinear dynamics in BALs, we use a 2(space)+1(time) dimensional traveling wave (TW) model [7, 8, 9] and the EO-solver `BALaser` [10] developed at the Weierstrass Institute in Berlin. In this model, we take into account only the optical field and carrier dynamics within the thin active zone of the laser along the lateral and longitudinal coordinates x and z, see Fig. 1(b). A set of effective model parameters represents the influence of the vertical device structure. In the computational domain, we distinguish different areas according to the positions of the electrical contacts, etched trenches, or unbiased regions. The following paraxial TW equations govern the spatiotemporal dynamics of the optical field $E(x,z,t) = \begin{pmatrix} E^+ \\ E^- \end{pmatrix}$ with E^+ and E^- denoting the slowly varying complex amplitudes of the counter-propagating optical fields:

$$
\begin{aligned}
&\tfrac{n_g}{c_0}\partial_t E = \left[\begin{pmatrix} -\partial_z & -i\kappa(x,z) \\ -i\kappa(x,z) & \partial_z \end{pmatrix} - \tfrac{i}{2\bar{n}k_0}\partial_x^2 - i\beta(x,z,t) - \tfrac{\mathcal{D}}{2}\right] E + F_{sp},\\
&\mathcal{D}E = \bar{g}(x,z)\,(E-p)\,, \quad \partial_t p = \bar{\gamma}(x,z)(E-p) + i\bar{\omega}(x,z)p,\\
&\beta = k_0\left[\tilde{n}_0(x,z) - \sqrt{\sigma_N N} + \tilde{n}_T(x,z)\right] + i\tfrac{g(N,\|E\|^2)-\alpha_0(x,z)-f_N N-\alpha_{2P}\|E\|^2}{2},\\
&g = \tfrac{g'(x,z)\ln\left(\frac{\max(N,N_0)}{N_{tr}}\right)}{1+\varepsilon_G\|E\|^2}, \quad \begin{pmatrix} -1 \\ \sqrt{R_0} \end{pmatrix}\cdot E(x,0,t) = \begin{pmatrix} \sqrt{R_l} \\ -1 \end{pmatrix}\cdot E(x,l,t) = 0,
\end{aligned}
\tag{1}
$$

with $\|E\|^2 = E \cdot E$ and $\eta \cdot \zeta = \sum_j \eta^{j*} \zeta^j$ being a standard dot product of two vectors. n_g, c_0, κ, $k_0 = 2\pi/\lambda_0$, $\bar{n}$, and F_{sp} are the group velocity index, the speed of light in vacuum, the field coupling factor in the presence of Bragg gratings, the free-space central wavenumber (λ_0: central wavelength), the reference refractive index, and the Langevin noise term, respectively. The local photon density $\|E\|^2$ is related to the local field power density P (measured in W/m^2) through the relation $P = \frac{hc_0^2}{\lambda_0 n_g}\|E\|^2$ (h: Planck constant, e: elementary charge). The linear operator $\mathcal{D}$ models the material gain dispersion in Lorentzian approximation with $\bar{g}$, $\bar{\gamma}$, and $\bar{\omega}$ denoting the amplitude, the half-width at the half height, and the relative gain peak frequency detuning, respectively. The complex propagation factor β accounts for background-, free carrier-, and two-photon absorption α_0, $f_N N$, and $\alpha_{2P}\|E\|^2$ [14], for an initially induced refractive index profile (etched trenches, for example) $\tilde{n}_0$, electronic and thermal corrections of the index $\sqrt{\sigma_N N}$ and $\tilde{n}_T$ (subject of this paper), as well as for the material gain g which depends on the local carrier density $N(x, z, t)$ and takes into account nonlinear gain compression. Parameters R_0 and R_l are the field intensity reflection coefficients of the diode facets at $z = 0$ and $z = l$ (l: the length of the BAL). If needed, the longitudinal boundary conditions can be extended by additional terms representing optical injection or feedback from an external cavity [9]. At the lateral borders of the (sufficiently broad) computational domain, numerical method-induced periodic conditions are imposed. In our simulations, just before these borders, we introduce artificial absorbing regions, see Fig. 1(b), which further suppress reinjection of the optical fields to the computational domain through the lateral borders.

The diffusive rate equation

$$\partial_t N = \partial_x(D_N \partial_x N) + \tfrac{j_{az}(x,z,t)}{ed} - \left[\tfrac{N}{\tau_N} + BN^2 + CN^3\right] - \tfrac{c_0}{n_g}\Re[E \cdot (g - \mathcal{D})E] \tag{2}$$

governs the dynamics of the carrier densities. d is the depth of the active zone, whereas D_N and j_{az} are carrier diffusion and injected current density at the active zone ($y \in AZ$), respectively:

$$D_N = D_N(N, \partial_N \varphi_{az}), \qquad j_{az}(x, z_0, t_0) = -\sigma_p(x, y, z_0)\partial_y \varphi(x, y, z_0, t_0)|_{y \in AZ},$$

Whereas the carrier-dependent voltage at the active zone is a known function of the carrier density, $\varphi_{az} = \varphi_{az}(N(x, z_0, t_0))$, to determine j_{az} for each z_0 and t_0 we need to solve the Laplace problem

$$\begin{aligned} &\nabla_{x,y} \cdot (\sigma_p(x, y, z_0)\nabla_{x,y}\varphi(x, y, z_0, t_0)) = 0, \quad (x, y) \in \Omega_{cs}, \\ &\varphi|_{\Gamma_c} = U, \quad \varphi|_{\Gamma_{az}} = \varphi_{az}(x, z_0, t_0), \quad \partial_n \varphi|_{\Gamma_{cs} \setminus (\Gamma_{az} \cup \Gamma_c)} = 0, \end{aligned} \tag{3}$$

for the quasi-Fermi potential $\varphi(x, y, z_0, t_0)$ in the corresponding lateral/vertical (x/y) cross-section [black-framed region Ω_{cs} in Fig. 1(c)] of the BAL device [11, 12]. Here, the piecewise constant function $\sigma_p(x, y, z_0)$ is the electrical conductivity of p-doped materials within the domain Ω_{cs}, the function φ and the flux $\sigma_p \partial_n \varphi$ are continuous at the material interfaces, Γ_{cs}, Γ_c, and Γ_{az} denote the whole outer border of Ω_{cs} and the parts of this border located at the electrical contact and the active zone, respectively, whereas U is the applied voltage at the contact. For more details on the model, the laser diode structure considered below, and typical parameters, see Refs. [12, 15].

3 Thermal model

A HT model for BALs should take into account the heat spreading in the whole device and, in general, is given by a (3+1)-dimensional heat conduction equation. However, due to the strongly differing time scales and limited computing resources, such a model is not applicable to the study of the thermal-electrooptical dynamics in BALs. For this reason, we introduce two main simplifications.

First, since the characteristic distances in the longitudinal (z) and transverse (x/y) directions differ by at least ten times, we neglect the heat diffusion in z direction. The dynamic heat conduction equation for each fixed z_0, in this case, reads as

$$c_L(x,y,z_0)\partial_t T = \nabla_{x,y}\cdot(\kappa_L(x,y,z_0)\nabla_{x,y})T + s(x,y,z_0,t).$$

The temperature distribution $T(x,y,z_0,t)$ and the heat flux $\kappa_L\partial_n T$ preserve the continuity at the interfaces between different materials and satisfy the boundary conditions

$$\left[\kappa_L\partial_n T + \tfrac{T-T_{hs}}{r_{th}}\right]\Big|_{(x,y)\in\Gamma_{hs}} = \partial_n T|_{(x,y)\in\Gamma\setminus\Gamma_{hs}} = 0, \quad (x,y)\in\Omega, \tag{4}$$

where Γ and Γ_{hs} are the border of the whole domain Ω and the part of this border at the heat sink [lower or/and upper border of Ω in Fig. 1(c)], respectively. Coefficients c_L and κ_L are thermal capacity and conductivity, respectively, T_{hs} and r_{th} are temperature and thermal resistance at the heat sink. Function s is the heat source which, following Ref. [13], we write as a sum of four different parts, s_{Joule}, s_{abs}, s_{rec}, and s_{def}, representing Joule, absorption, non-radiative carrier recombination, and quantum defect heating sources, respectively:

$$\begin{aligned}
s_{Joule} &= \delta_{[(x,y)\in\Omega_{cs}]}\tfrac{\|\vec{j}\|^2(x,y,z_0,t)}{\sigma_p(x,y,z_0)},\\
s_{abs} &= \left(\delta_{[y\in AZ]}f_N N + \delta_{[y\notin AZ]}d\,\alpha(x,y,z_0)\Phi^2(y)\right)P,\\
s_{rec} &= \delta_{[y\in AZ]}\,e\,\varphi_{az}[\tfrac{N}{\tau_N} + BN^2 + CN^3],\\
s_{def} &= \delta_{[y\in AZ]}\,\max\{g(N,\|E\|^2)(\tfrac{e\lambda_0}{hc_0}\varphi_{az}-1),0\}P.
\end{aligned}$$

Here, the piecewise constant α represents an effective linear absorption of different materials, the step-function $\delta_{[\zeta]}$ is equal to 1 when the condition ζ is fulfilled and is 0 otherwise. Seeking to avoid a computationally expensive estimation of the total current flux $\|\vec{j}\| = \sigma_p\|\nabla_{x,y}\varphi\|$ within the whole cross-section domain Ω_{cs} at each position z_0 and time t, in the following, we exploit a simple approximation

$$\|\vec{j}(x,y,z_0,t)\| \approx \delta_{[((x,y)\in\Omega_{cs})\&(x\in\Pi_x\Gamma_c)]}\left|\frac{U-\varphi_{az}(x,z_0,t)}{\int_{(x,y)\in\Omega_{cs}}\sigma_p^{-1}(x,y,z_0)dy}\right|,$$

which one can easily derive from the CS-problem (3) with the neglected lateral current spreading, $\partial_x\varphi = 0$. The notation $\Pi_x\Gamma_c$ above denotes the projection of the electrical contact position Γ_c onto the lateral x- axis and, therefore, represents those (x,y) which are below or above the electrical contact. After this replacement, the time dependence of all heat sources is determined by the y-independent functions $\|E\|^2$ (proportional to P), N, and φ_{az} which can be accessed when solving the EO model (1)-(3).

The huge difference in the time scales of optoelectronic and thermal processes motivates our second simplification. Namely, a proper calculation of the heat-transport evolution would require computations of the transients over several microseconds, whereas the final operating state in the electro-optical model usually can be achieved in less than ten nanoseconds. For this reason, within up to several nanosecond long transients ($t\in[t_0-\tau,t_0]$, $\tau\sim$ns), we ignore the temperature evolution and look for temperature distributions $\bar{T}(x,y,z_0)$ averaged over this time interval instead. The static HT problem for $\bar{T}$ at each z_0 reads

$$\nabla_{x,y}\cdot(\kappa_L(x,y,z_0)\nabla_{x,y})\bar{T}(x,y,z_0) + \langle s\rangle_\tau(x,y,z_0) = 0, \quad (x,y)\in\Omega, \tag{5}$$

where $\bar{T}$ satisfies the boundary conditions (4) and $\langle\chi\rangle_\tau = \frac{1}{\tau}\int_{t=t_0-\tau}^{t_0}\chi(t)dt$ denotes the time average of the function $\chi(t)$ over the time interval $[t_0-\tau,t_0]$. The time-averaged heat source $\langle s\rangle_\tau$ in Eq. (5) is

generated using different functions of fields, carriers, Fermi potentials, and current injection (denoted by ν_j below) which can be collected when solving the EO-model during the time interval $[t_0 - \tau, t_0]$:

$$\langle s \rangle_\tau(x, y, z_0) = \sum_j \iota_j(x, y, z_0) \langle \nu_j \rangle_\tau(x, z_0).$$

Functions ι_j in the formula above depend on the material and model parameters, the geometry of the device, and the initially precalculated static operating vertical mode intensity $\Phi^2(y)$, see the black curve in Fig. 2(a).

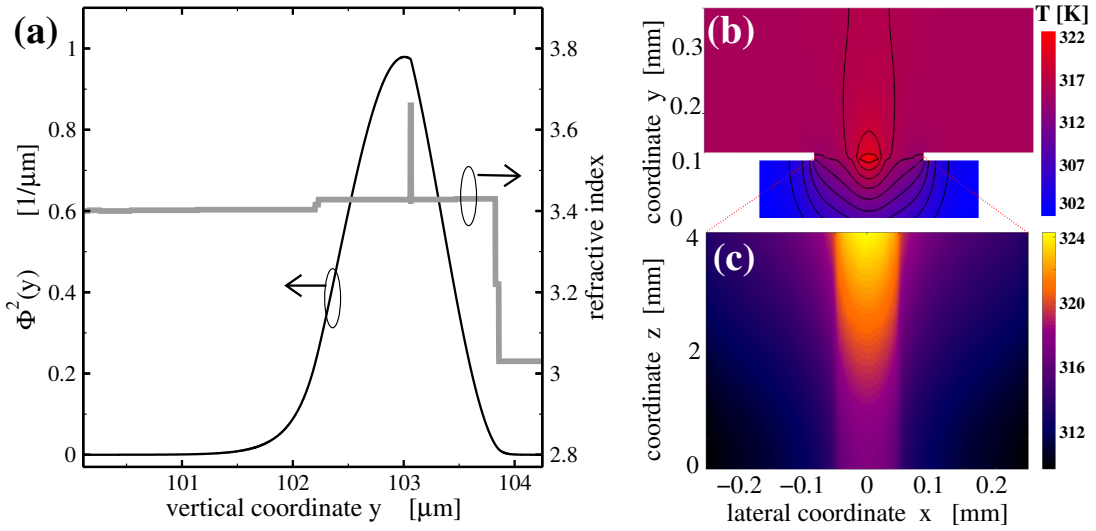

Figure 2: (a): vertical distributions of the optical mode intensity (black) and the refractive index (thick gray). (b): typical calculated distribution of time-averaged temperature $\bar{T}(x, y, z_0)$ at a single vertical-lateral cross-section of the BAL. (c): calculated distribution of the temperature $\bar{T}_{az}(x, z)$ at the position of the active zone.

Typical calculations of the temperature distribution $\bar{T}$ within a single cross-section of the 4 mm long and 90 μm wide HP-BAL operating at ~ 13 W are shown in Fig. 2(b). The three-dimensional distribution $\bar{T}(x, y, z_0)$ obtained after resolving the 2D-problem (5) for all domain discretization-induced laser cross-sections $z = z_0$ is used for the determination of the temperature $\bar{T}_{az}$ within the active zone layer [see Fig. 2(c)] and the thermally-induced refractive index correction $\tilde{n}_T$:

$$\bar{T}_{az} = \tfrac{1}{d}\textstyle\int_{y\in AZ} \bar{T}(x, y, z_0)dy, \quad \tilde{n}_T = \frac{\int n'_T(x,y,z_0)\frac{\tilde{n}_0(x,y,z_0)}{\bar{n}}\Phi^2(y)\bar{T}(x,y,z_0)dy}{\int \Phi^2(y)dy}.$$

Here, the piecewise constant distribution $\tilde{n}_0$ is defined by the refractive indices of corresponding materials [e.g., grey line in Fig. 2(a)] and n'_T denotes the change of these indices with changing temperature. Whereas $\bar{T}_{az}$ is used for the definition of several parameters of the EO model, $\tilde{n}_T$ is of crucial importance when seeking to obtain proper characteristics of the stimulated emission.

4 Numerical algorithm

When performing comprehensive simulations of the dynamics in HP BALs, we solve numerically the dynamic TW model (1), (2), the static CS problems (3), and the static HT problems (4), (5). Each of these three models is resolved by the corresponding solver. The interaction of all these models and solvers is schematically represented in Fig. 3(a).

For numerical integration of the TW model, we exploit the software kit `BALaser` [10]. The numerical algorithm is based on the split-step method for the field equations (1) and the finite difference approximations of the carrier rate equations (2). The temporal-longitudinal propagation and the lateral diffraction of the fields in (1) are treated by means of finite difference schemes and a fast Fourier transform algorithm, respectively. For the acceleration of time-consuming calculations, the numerical algorithm was parallelized using distributed-memory paradigm. As a consequence, instead of ~ 2 hours required for simulation of 1-ns long transients of a typical BAL using the single process on a single core of our server, we perform the same simulations exploiting 30 processes in about 5 minutes. More details on the algorithms used to solve the TW model can be found in Refs. [8, 9].

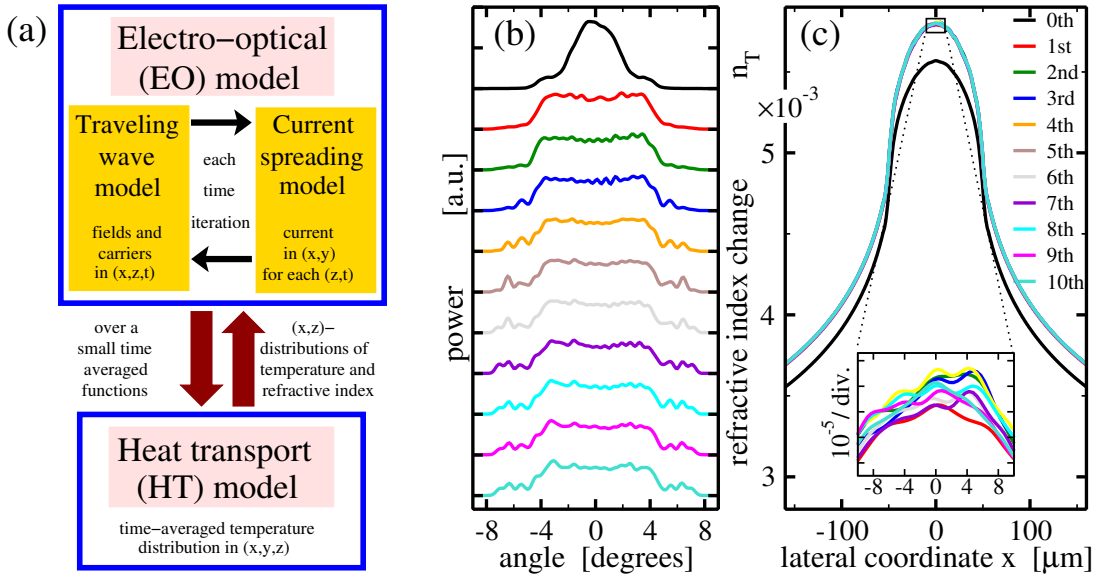

Figure 3: (a): schematics of the HP BAL simulator. (b) and (c): evolution of the time-averaged far-fields and thermally-induced refractive index change profiles $\tilde{n}_T(x)$ at the front facet, respectively, during the iterative application of EO- and HT-solvers for a 4 mm-long HP-BAL device having a $90\ \mu$m-wide contact stripe with ~ 13 W emission power. Solid black curves correspond to the initial iteration step where the temperature distribution was not yet accounted for by the EO solver.

Once dealing with the CS problem (3), we use the finite volume discretization based schemes and the software toolkit pdelib [16] developed at the Weierstrass Institute in Berlin. Since the TW and CS solvers should exchange information at each time iteration step, the consequent multiple application of the CS solver numerically is too expensive. For example, during 1-ns transient simulations of typical BALs, one needs to exploit the CS-solver about 10 million times! For this reason, we use the linearity of the CS problem and the Green-function-like approach. Within an initialization step of our combined EO-solver [see Fig. 3(a)], we apply the CS solver for the construction of a $N_x \times (N_x{+}1)$-dimensional matrix $\mathcal{M}$ (N_x: number of the equidistant lateral mesh points x_i used when solving the TW model) consisting of $(N_x{+}1)$ "elementary" discrete injected current density N_x-dimensional vector-functions j^i_{az}, $i = 0, \ldots, N_x$, corresponding to the CS problems with elementary (discrete) boundary conditions $(U, \varphi_{az}) = (1, 0)$ in the case of $i = 0$, and $(U, \varphi_{az}) = (0, \delta_{[x=x_i]}(x))$ for $i = 1, \ldots, N_x$. Later, the multiplication of $\mathcal{M}$ with the actual (instantly changing) $(N{+}1)$-dimensional vector $(U, \varphi_{az})^T$ gives us the required function j_{az}. To reduce the number of ($\sim N_x^2$) arithmetic operations required by the full matrix-vector multiplication, we ignore the majority of small off-diagonal elements of $\mathcal{M}$. For more details on the applied algorithms for the CS problem, see Ref. [11].

For the numerical solution of the HT problem (4), (5), we use the toolkit pdelib [16] again. The nu-

merical method is based on a finite volume space discretization, resulting in a sparse linear system of equations $A_h T_h = -s_h$ (A_h, s_h, T_h: discrete approximations of the differential operator, source, and temperature, respectively) which is solved via the LU factorization $A_h = L_h U_h$ into easily invertible upper and lower triangular factors, s.t. $T_h = -U_h^{-1} L_h^{-1} s_h$ [17]. Since the differential operator in Eq. (5) is linear, and most of the considered BALs have a single or only a few different cross-sections, the same LU factorization can be applied w.r.t. multiple source functions s_h corresponding to different values of z. For typical laser structures, the calculation time required by the HT-solver does not exceed 1-2 minutes (compare to at least ~ 30 minutes needed for standard 5-ns long transient simulations of the same BALs by the EO-solver). Typical calculated heat distributions within the lateral-vertical cross-section and the active layer of the HP-BAL device are shown in Figs. 2(b) and (c), respectively.

The EO- and HT-solvers are self-consistently coupled using the following iterative procedure:

(0) In this initialization step, we perform ≥ 5 ns long transient simulations of the BAL with the dynamic EO-solver using given temperature and refractive index distributions $\bar{T}_{az}(x,z)$ and $\tilde{n}_T(x,z)$, or setting $\bar{T}_{az} = T_{hs}$ and $\tilde{n}_T = 0$ if these distributions are not provided.

(1) Our EO simulations provide time-averaged distributions $\langle \|E\|^2 \rangle_\tau(x,z)$ (which are proportional to $\langle P \rangle_\tau(x,z)$), $\langle N \rangle_\tau(x,z)$, and $\langle \varphi_{az} \rangle_\tau(x,z)$. All these functions together with the originally supplied mode intensity profile $\Phi^2(y)$ are used for the construction of the (time-averaged) heat source function $\langle s \rangle_\tau(x,y,z)$.

(2) The static HT-solver uses the estimated source $\langle s \rangle_\tau$. From the obtained 3-dimensional temperature distribution $\bar{T}(x,y,z)$, we construct 2-dimensional distributions $\bar{T}_{az}(x,z)$ and $\tilde{n}_T(x,z)$ in the active layer.

(3) We perform ≥ 5 ns long transient simulations of the BAL with the dynamic EO-solver using the distributions $\bar{T}_{az}(x,z)$ and $\tilde{n}_T(x,z)$ and proceed to the step (1) of our iterative procedure.

5 Example

To illustrate the performance of our iterative coupling of EO- and HT-solvers, we have simulated the dynamics in a 4 mm-long HP-BAL device having a $90\,\mu$m-wide contact stripe with ~ 13 W emission power, considered earlier in Refs. [12, 15]. Different curves in Figs. 3(b) and (c) represent calculated far fields and distributions $\tilde{n}_T(x,z)$ (estimated at the front facet, $z = l$) obtained during different iteration steps.

When first initiating the EO-solver, the considered BAL is switched off, whereas the distributions $\bar{T}_{az}$ and $\tilde{n}_T$ are set to constants T_{hs} and 0, respectively. Far-fields averaged over the last 2 ns of the first simulated 5 ns transients are shown by the upper solid black curve in Fig. 3(b). In the absence of a thermally induced refractive index profile n_T, the far-field divergence is relatively small. In the next step of the algorithm, the HT-solver exploits the time-averaged distributions calculated by the EO-solver for the definition of $\bar{T}_{az}$ and $\tilde{n}_T$, see the black curve in panel (c) of the same figure. Next, during the consequent 5 ns transient calculations the EO-solver accounts for the previously defined $\bar{T}_{az}$ and $\tilde{n}_T$, whereas the HT-solver is using the heat sources specified by the just updated time averaged distributions. Panel (c) shows how the initial correction slightly enhances the profile of $\bar{n}_T$, whereas the following iterations imply only small additional deviations (order 10^{-5}) of $\bar{n}_T$, see inset of Fig. 3(c). The far-fields change further during this iterative procedure. Once inspecting the far-field profiles obtained during the consequent iterations [curves counted from top to down in Fig. 3(b)], one

can clearly distinguish growing emission around $\pm 6^\circ$. After approximately seven iterations (40 ns after switching on the laser), these distributions converge.

In conclusion, we discussed an efficient coupling of the dynamic EO- and the static HT-solvers for BALs. The calculation time used by the HT solver usually is less than 10% of the time required by the EO solver. The application of the HT-solver allows a self-consistent estimation of the temperature distribution and the thermal lensing within the active zone of the device, which is crucial for proper simulation of the emission from CW HP-BALs by the EO-solver.

References

[1] R. Diehl, *High-Power Diode Lasers: Fundamentals, Technology, Applications* (Springer, Berlin, 2000)

[2] H. Wenzel, "Basic aspects of high-power semiconductor laser simulation," IEEE J. of Select. Topics in Quantum Electron. **19**, 1-13 (2013)

[3] L. Borruel, S. Sujecki, P.M.D. Moreno, J. Wykes, M. Krakowski, B. Sumpf, P.A. Sewell, S.C. Auzanneau, H. Wenzel, D. Rodriguez, T.M. Benson, E.C. Larkins, I. Esquivias "Quasi-3-D simulation of high-brightness tapered lasers," *IEEE J. Quantum Electron.*, **40**(3), 463-472 (2004)

[4] Y. Champagne, S. Mailhot, and N. McCarthy, "Numerical procedure for the lateral-mode analysis of broad-area semiconductor lasers with external cavity," *IEEE J. Quantum Electron.*, **31**, 795-810 (1995)

[5] S. Blaaberg, P.M. Petersen, and B. Tromborg, "Structure, stability, and spectra of lateral modes of a broad-area semiconductor laser," *IEEE J. of Quantum Electron.*, **43**, 959-973 (2007)

[6] T. Tachikawa, S. Takimoto, R. Shogenji, and J. Ohtsubo, "Dynamics of Broad-Area Semiconductor Lasers With Short Optical Feedback," *IEEE J. Quantum Electron.*, **46**, 140-149 (2010)

[7] M. Spreemann, M. Lichtner, M. Radziunas, U. Bandelow, and H. Wenzel, "Measurement and simulation of distributed-feedback tapered master-oscillators power-amplifiers," IEEE J. Quantum Electron., **45**, 609-616 (2009)

[8] M. Radziunas and R. Čiegis, Effective numerical algorithm for simulations of beam stabilization in broad area semiconductor lasers and amplifiers. *Math. Model. and Anal.*, **19**, 627-644 (2014)

[9] M. Radziunas, "Modeling and simulations of broad-area edge-emitting semiconductor devices," *The Int. J. of High Perform. Comp. Appl.*, **32**(4), 512-522 (2018)

[10] "BALaser: a software tool for simulation of dynamics in Broad Area semiconductor Lasers," *http://www.wias-berlin.de/software/BALaser*

[11] M. Radziunas, A. Zeghuzi, J. Fuhrmann, T. Koprucki, H.-J. Wünsche, H. Wenzel, and U. Bandelow, "Efficient coupling of the inhomogeneous current spreading model to the dynamic electro-optical solver for broad-area edge-emitting semiconductor devices," *Optical and Quantum Electronics*, **49**, 332 (2017)

[12] A. Zeghuzi, M. Radziunas, H. Wenzel, H.-J. Wünsche, U. Bandelow, and A. Knigge, “Modeling of current spreading in high-power broad-area lasers and its impact on the lateral far field divergence,” *SPIE Proceedings Series*, **10526**, 105261H (2018)

[13] S. Rauch, H. Wenzel, M. Radziunas, M. Haas, G. Tränkle, and H. Zimer, “Impact of longitudinal refractive index change on the near-field width of high-power broad-area diode lasers,” *Appl. Phys. Lett.*, **110**(26) 263504 (2017)

[14] A. Zeghuzi, M. Radziunas, A. Klehr, H.-J. Wünsche, H. Wenzel, and A. Knigge, “Influence of nonlinear effects on the characteristics of pulsed high-power broad-area distributed Bragg reflector lasers,” *Opt. and Quantum Electron.*, **50**, 88 (2018)

[15] P. Crump, G. Erbert, H. Wenzel, C. Frevert, C.M. Schultz, K.-H. Hasler, R. Staske, B. Sumpf, A. Maaßdorf, F. Brugge, S. Knigge, and G. Tränkle, “Efficient High-Power Laser Diodes,” *IEEE J. of Sel. Topics in Quantum Electron.*, **19**(4), 1501211 (2013)

[16] J. Fuhrmann, T. Streckenbach et al., “pdelib: A finite volume and finite element toolbox for PDEs,” *http://pdelib.org*

[17] T. A. Davis, UMFPACK V4.3, ACM TOMS, **30**(2), 196-199 (2004)